SUPPLEMENTAL EVALUATION OF GEOPHYSICAL INFORMATION USED TO DETECT AND CHARACTERIZE BURIED VOLCANIC FEATURES IN THE YUCCA MOUNTAIN REGION

Prepared for

U.S. Nuclear Regulatory Commission
Contract NRC–02–02–012

Prepared by

John A. Stamatakos
Saurav Biswas
Mark Silver

Center for Nuclear Waste Regulatory Analyses
San Antonio, Texas

August 2007

EXECUTIVE SUMMARY

The probability of future igneous activity affecting the potential repository site at Yucca Mountain, Nevada, is addressed in models of the total system performance assessment. Uncertainties in igneous activity probability affect risk calculations linearly such that each order of magnitude increase in probability increases risk by an order of magnitude. In 2004, the U.S. Department of Energy (DOE) reconvened an expert elicitation panel to reassess the probability of an igneous event disrupting the potential repository for high-level nuclear waste at Yucca Mountain. The Probabilistic Volcanic Hazard Assessment-Update (PVHA-U)[1] supersedes the original DOE probabilistic Hazard Assessment (PVHA),[2] which was concluded in 1996. The goal of this PVHA-U is to characterize the spatial and temporal distributions of future igneous events and associated geometries and characteristics of intrusive and extrusive igneous activity at Yucca Mountain for both a 10,000- and 1-million-year period of performance. Results of the updated assessment will be probability distributions defining the annual frequency of intrusive and extrusive igneous events that can be combined with consequence studies in a performance assessment used to assess risk.

To support the expert elicitation, the DOE sponsored a high-resolution aeromagnetic survey of the Yucca Mountain region. The survey was conducted using a helicopter with an average sensor elevation of 40–50 m [131–164 ft] above terrain. Based on the resulting anomaly map, DOE identified a subset of seven anomalies for additional testing. The DOE drilled these seven anomalies to determine whether basaltic igneous features buried in the subsurface were the sources of the anomalies. The DOE encountered basalt in four of the seven boreholes. Basalt samples from those four boreholes were cored for additional analyses, including radiometric age determinations and mineral identification. Staff obtained basalt core samples from the DOE Sample Management Facility from which petrologic, magnetic, and paleomagnetic data were obtained. The magnetic data provided additional constraints for two-dimensional geophysical models of the anomalies.

These geophysical models help staff assess and rank identified anomalies in terms of how likely the anomalies represent basaltic features in the subsurface. This ranking will also be used by staff to evaluate uncertainties in probability models DOE developed in the PVHA-U. Analyses provided in this report supplement and update the initial evaluation of aeromagnetic data provided in the 2002 CNWRA report “Evaluation of Geophysical Information Used to Detect and Characterize Buried Volcanic Features in the Yucca Mountain Region” by Brittain Hill and John Stamatakos. In the 2002 report, Hill and Stamatakos concluded that there may be twice as many basaltic volcanoes in the Yucca Mountain region than considered in the original 1996 DOE hazard assessment. These additional buried volcanoes could potentially lead to a tenfold increase in probability estimates for igneous activity at Yucca Mountain.

The new DOE analyses have reduced the overall uncertainty in the number of past events. Specifically, many of the anomalies that were previously ranked as having a high or medium likelihood of being the result of buried basalt are now confirmed buried basaltic features while

[1]The phrase “Probabilistic Volcanic Hazard Assessment-Update” (PVHA-U) is used repeatedly throughout this document; therefore, for ease of reading, the acronym PVHA-U has been used.

[2]The phrase “Probabilistic Volcanic Hazard Assessment” (PVHA) is used repeatedly throughout this document, therefore; for ease of reading, the acronym PVHA has been used.

several anomalies ranked as having a low likelihood of being buried basalt are now confirmed as being the result of faulted tuff. Moreover, the aeromagnetic data and drilling program have identified previously unknown Miocene basalt buried in Fortymile Wash.

The new DOE information and analyses also support the hypothesis that past volcanism in the Yucca Mountain region is temporally clustered. The most active of these temporal clusters was one that occurred between 3.6 and 4.7 million years ago, in which at least 12 to 17 volcanoes formed. This leads to an episodic recurrence rate of 11 to 16 volcanoes per million years, which is substantially greater than the longer term average rate of about 5 volcanoes per million years and an order of magnitude greater than the 1 to 3 volcanoes per million years in the original 1996 DOE assessment. Additional temporal clusters are recognized for the period between about 9 and 11.2 million years ago and one between 80,000 and 1 million years ago. Based on these data, it appears that temporal clustering is an important feature of the Yucca Mountain system that should be accounted for in volcanic probability models.

In addition to temporal clustering, new data and modeling results from the drill core at anomaly A reveal an accumulation of basalt that appears to be a very thick intrusion or sill rather than a buried volcanic lava flow or cone. This is the first documented evidence of a voluminous basaltic sill in the Crater Flat structural basin. The presence of a sill raises the possibility that, in addition to existing igneous activity scenarios in which a basaltic dike intersects repository drifts or a volcanic conduit forms thorough the repository, a basaltic sill could form within or beneath the potential Yucca Mountain repository.

Finally, the new DOE data coupled with the magnetic and petrologic studies documented in this report improve resolution of buried basaltic volcanic features and thereby reduce but do not eliminate uncertainties in spatial and temporal recurrence rates. Magnetic data alone cannot differentiate basalt from faulted tuff in areas with extensive tuff outcrops. Magnetic properties of the tuffs and basalts are comparable, and without additional information, magnetic anomalies arising from fault to tuff or basalt appear quite similar. This ambiguity was apparent in interpretations of anomaly Q, which the U.S. Geological Survey ranked as unlikely to be buried basalt. The DOE drill hole at anomaly Q encountered basalt at 140–163 m [459–535 ft]. Thus, areas with faulted tuff at or near the surface could contain additional, undetected basalt. This “present but undetected” designation adds uncertainty to volcano counts used in probability studies. The analyses provided in the 2002 Hill and Stamatakos report remain valid methods for staff to evaluate the potential for present but undetected volcanoes.

CONTENTS

FIGURES

TABLES

ACKNOWLEDGMENTS

This report was prepared to document work performed by the Center for Nuclear Waste Regulatory Analyses (CNWRA) for the U.S. Nuclear Regulatory Commission (NRC) under Contract No. NRC–02–02–012. The activities reported here were performed on behalf of the NRC Office of Nuclear Material Safety and Safeguards, Division of High-Level Waste Repository Safety. The report is an independent product of the CNWRA and does not necessarily reflect the views or regulatory position of the NRC.

This reports builds on work and analyses originally documented in Hill and Stamatakos (2002), by examining the results of the U.S. Department of Energy (DOE) magnetic anomaly mapping and drilling program conducted in the last five years. The supplemental analyses and evaluations of magnetic and related data in this report benefitted substantially from discussions with Brittain Hill, Phillip Justus, John Trapp, and Nancy Adams. H. Lawrence McKague, Alan Morris, and David Ferrill also helped our interpretations of geological, geophysical, and tectonic-magmatic setting of Yucca Mountain. We thank Deborah Waiting and Shannon Colton for their assistance with the Geographic Information System and data processing and Sharon Odam, Beverly Street, and Lauren Mulverhill for editorial support and report preparation. Finally, we are grateful for the technical review by Nancy Adams and programmatic review by Gordon Wittmeyer, which greatly improved the quality and clarity of the information in this report.

QUALITY OF DATA, ANALYSES, AND CODE DEVELOPMENT

DATA: The CNWRA data contained in this report meet the quality assurance requirements described in the Geosciences and Engineering Division Quality Assurance Manual. Data from other sources are identified by reference to their source. The respective sources of these non-CNWRA data should be consulted to determine the level of quality assurance. Data used to support conclusions in this report taken from documents published by DOE contractors and supporting organizations were also generated under the quality assurance program developed by the DOE for the Yucca Mountain Project.

ANALYSES AND CODES: Mapping and modeling of geophysical data was performed using the Oasis MONTAJ™ Version 6.3.1 (6G) (2006), a commercial software code from Geosoft, Inc. and GM-SYS© Version 4.8.45b, a commercial software code from Northwest Geophysical Association (2001). These are maintained in accordance with CNWRA Technical Operating Procedure TOP–018. Details of the specific procedures used to model the magnetic data in this report are contained in scientific notebook 758E.

References:

Geosoft, Inc. "Oasis MONTAJ™." Version 6.3.1 (6G). Toronto, Ontario, Canada: Geosoft, Inc. 2006.

Hill, B.E. and J.A. Stamatakos. "Evaluation of Geophysical Information Used to Detect and Characterize Buried Volcanic Features in the Yucca Mountain Region." San Antonio, Texas: CNWRA. 2002.

Northwest Geophysical Association. "GM-SYS©." Version 4.8.45b. Corvallis, Oregon: Northwest Geophysical Association. 2001.

1 INTRODUCTION

1.1 Background

Volcanic hazards are a potential concern to the safe disposal of nuclear waste at Yucca Mountain, Nevada, because of the location of the potential repository within a geologically active basaltic volcanic field. In the last 11 million years, at least 40 basaltic vents have formed within a radius of approximately 50 km [31 mi] of Yucca Mountain. Within the last million years, six cinder cones formed within a 20-km [12.5-mi] radius of Yucca Mountain (e.g., Fleck, et al., 1996). Geophysical studies have also shown that additional volcanic features such as vents, lava flows, dikes, and possibly sills may be buried in the alluvial basins surrounding Yucca Mountain or as intrusions within the thick accumulation of silicic volcanic strata that constitute much of the exposed bedrock of the region (e.g., Langenheim, 1995; Stamatakos, et al., 1997). Because of the potential for volcanic activity to disrupt waste packages and transport radionuclides to the surface, future basaltic igneous activity is considered in postclosure performance assessments. The U.S. Nuclear Regulatory Commission (NRC) Risk Insights Baseline Report, contained in the Integrated Issue Resolution Status Report (NRC, 2005), currently considers the probability of igneous activity as having high significance to waste isolation. Igneous event probability has been the focus of studies sponsored by the U.S. Department of Energy (DOE), NRC, State of Nevada, and the Electric Power Research Institute spanning the last three decades (e.g., CRWMS M&O, 2000a,b; Electric Power Research Institute, 2003; Ho and Smith, 1998; NRC, 2005).

The risk of igneous activity to repository performance is the product of the potential consequences of an igneous intrusion or volcanic conduit intersecting and damaging waste packages in the repository times the probability that one or both of these igneous processes will occur. Probability studies have focused on characterizing the location, age, and composition of relevant igneous features of past igneous events as a basis for probability estimates of future igneous activity. These probability studies rely on a wide range of information, including geological observations of nearby igneous features; geochemical and petrologic studies of regional basaltic systems; geophysical studies of the crust, lithosphere, and upper mantle; and studies of analog volcanic systems around the world.

Although these characteristics of the Yucca Mountain region basaltic system were thought to be reasonably well established by the mid-1990s, DOE concluded that sufficient uncertainties in data and models remained to warrant use of an expert elicitation to develop reliable estimates of the probability for future igneous activity, including incorporation of uncertainty. The 1995–1996 DOE probabilistic volcanic hazard assessment (PVHA)[1] resulted in a probability distribution of the annual frequency of a basaltic dike intersecting the repository that ranged from 1×10^{-10} to 1×10^{-7}, with a mean of 1.6×10^{-8} (CRWMS M&O, 1996). NRC regulations for disposal of high-level radioactive waste at Yucca Mountain (CFR Part 63) require that disruptive events with a likelihood of one chance in 10,000 over a 10,000-year period of performance (i.e., approximately 1×10^{-8}/yr) be included in the DOE performance assessment. The results

[1]The phrase “Probabilistic Volcanic Hazard Assessment” (PVHA) is used repeatedly throughout this document; therefore, for ease of reading, the acronym PVHA has been used.

of the DOE expert elicitation thus required DOE to consider igneous activity within their performance assessment.

A detailed aeromagnetic survey by the U.S. Geological Survey (Blakely, et al., 2000) revealed the possibility of 20 or more previously uncharacterized basaltic volcanoes that may be buried in the alluvial basins of Crater Flat, Jackass Flat, and the Amargosa Desert. Analyses of the Blakely, et al. (2000) data by Hill and Stamatakos (2002) and O'Leary, et al. (2002) showed that the uncertainties associated with the new aeromagnetic data coupled with new information about the regional tectonic setting translated into substantial uncertainties in estimates of future igneous activity at Yucca Mountain. Hill and Stamatakos (2002) evaluated 24 anomalies as potentially buried volcanic basalt. O'Leary, et al. (2002) identified 20 anomalies as possible basaltic volcanic features. In addition to the number of past volcanic events, the age and composition of these buried volcanoes could be different from recognized patterns of igneous activity, and this could fundamentally change the conceptual models of the geologic processes DOE experts relied on to explain the occurrence of basaltic igneous activity in this region for the last 11 million years. Based on the evaluation provided in Hill and Stamatakos (2002) and O'Leary, et al. (2002), NRC observed that current site information and available models showed that the 1995–1996 PVHA did not address current uncertainties in recurrence rate, and consideration of alternative models (Schlueter, 2002). DOE committed to update the 1995–1996 PVHA to confirm the licensing basis for characterization of the volcanic hazard for the potential Yucca Mountain repository (Ziegler, 2003). In 2004, DOE convened the Probabilistic Volcanic Hazard Assessment-Update (PVHA-U).[2] According to Coppersmith, et al. (2005), the PVHA-U assessments will include spatial distribution of igneous events, temporal distributions, and geometries and characteristics of future intrusive and extrusive events for both a 10,000-year and 1-million-year period of performance. The results of the PVHA-U will be a series of probability distributions defining the annual frequencies of intrusive and extrusive igneous events that can be combined with consequence studies in a performance assessment used to assess risk. DOE expects to complete the PVHA-U in 2008.

To support the expert elicitation data needs, DOE sponsored a new higher resolution, helicopter-borne aeromagnetic survey of the Yucca Mountain region and a borehole drilling program of selected anomalies based on the aeromagnetic survey results to better characterize the number, location, and age of buried volcanoes. The helicopter aeromagnetic survey was completed in 2004. It covered an area of 865 km^2 [334 mi^2] including Yucca Mountain and portions of Crater Flat, Jackass Flat, and the Amargosa Desert (Figure 1-1). The survey consisted of 16,000 km [9,942 mi] of east-west flight lines with a line spacing of 60 m [197 ft] and an instrument height of 40–50 m [131–164 ft] above the flat terrain.[3] Secondary tie lines were flown north-south, with a line spacing of 600 m [1,968 ft]. The survey flew a total-field cesium-vapor magnetometer yielding a resolution nearly equivalent to the previous ground magnetic surveys conducted over specific targets in the region (e.g., Connor, et al., 2000, 1997; Magsino, et al., 1998; Stamatakos, et al., 1997). The accuracy of the magnetic data was ±0.01 nT. Measurement locations are accurate to ±1 m [3.3 ft] horizontally and ±2 m [6.6 ft]

[2]The phrase "Probabilistic Volcanic Hazard Assessment-Update" (PVHA-U) is used repeatedly throughout this document; therefore, for ease of reading, the acronym PVHA-U has been used.

[3]Aeromagnetic data were obtained from Los Alamos National Laboratory FTP site with permission from the DOE. ftp://ees.lanl.gov/pub/ahc/YMP/Aeromag/FinalMagData-TraverseLines.zip and ftp://ees.lanl.gov/pub/ahc/YMP/Aeromag/FinalMagData-TieLines.zip

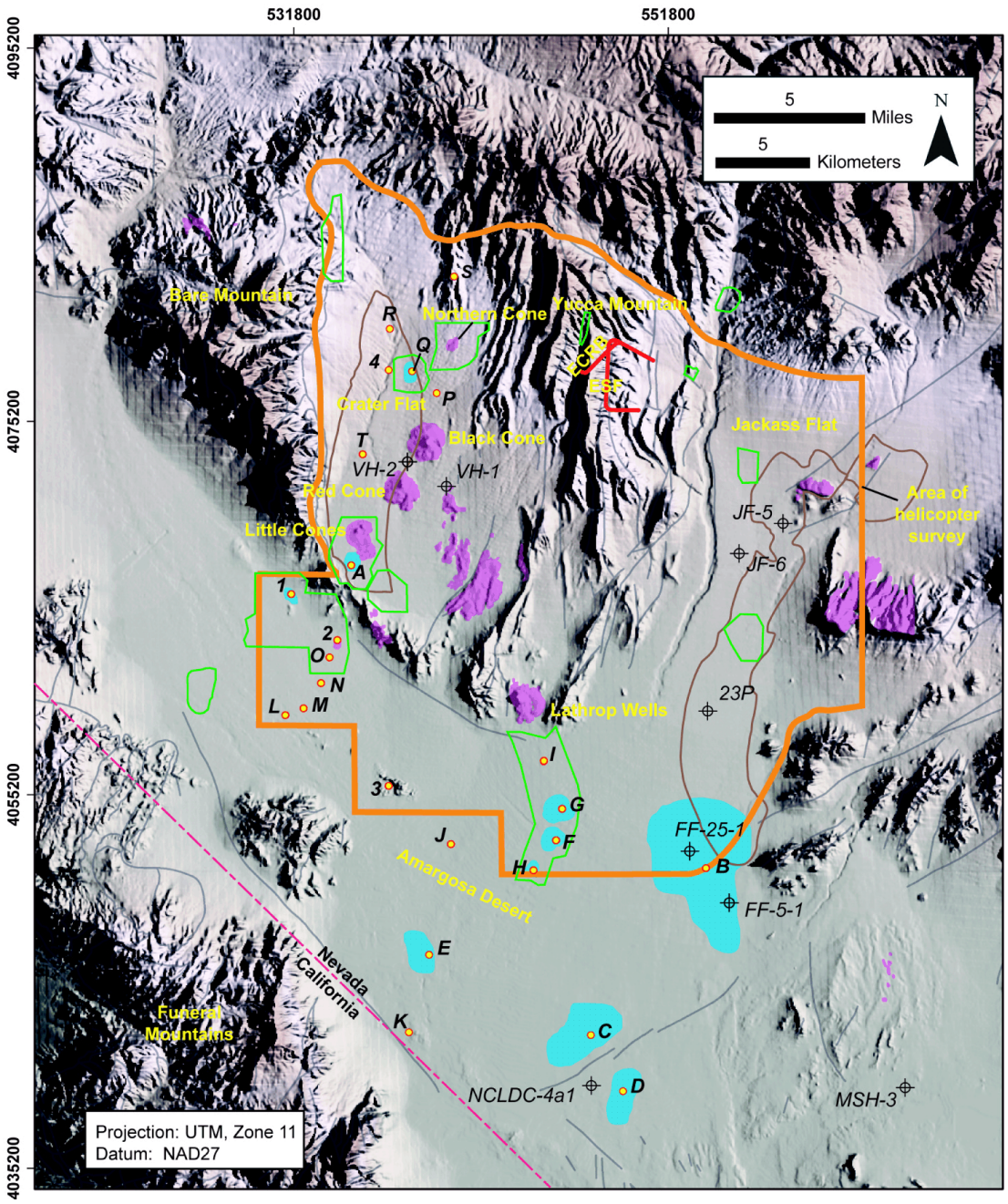

Figure 1-1. Location Map of Features Relevant to Igneous Activity Studies. Base Map Is a Colorized Shaded Relief Digital Elevation Model Based on 1 m [3.3 ft] Digital Elevation Data. Orange Outline Delineates the DOE Aeromagnetic Survey Area. Green Outlines Show Location of Center for Nuclear Waste Regulatory Analyses Ground Magnetic Surveys (Magsino, et al., 1998). Purple Shading Shows Exposures of Basalt. Blue Shading Shows Location of Buried Basalt Based on Aeromagnetic Data or Drilling Information.

vertically. The resulting magnetic anomaly map (Figure 1-2) revealed up to 33 features that were interpreted by Perry, et al. (2005) as buried volcanoes or faulted tuff bedrock (Perry, et al., 2006).

Based on the new aeromagnetic survey, DOE selected seven anomalies to be drilled and cored. DOE used three criteria to select the subset of seven anomalies. These were to (i) balance the low and high confidence anomalies provided in Hill and Stamatakos (2002) and O'Leary, et al. (2002); (ii) sample major clusters or alignments of anomalies; and (iii) examine a range of potential ages of basaltic features based on burial depth and magnetic polarity. The drilling program was completed in 2006. Of the seven anomalies drilled, four encountered basalt (Table 1-1).

Table 1-1. DOE Data From Boreholes*

Anomaly	Depth	Interpreted Anomaly Source	Ages (Ma)†	Notes
A	148–211 m [586–692 ft]	Basalt	10.08 ± 0.02 10.04 ± 0.02	Lack of flow features and thickness suggest the body may be a sill
Q	140–163 m [459–535 ft]	Basalt	11.07 ± 0.2 10.80 ± 0.5	Four lava flows separated by breccia and scoria
G	119–145 m [390–476 ft]	Basalt	3.74 ± 0.21 3.99 ± 0.22	Scoria at top and bottom of flow
JF5	77–94 m [253–308 ft]	Basalt	9.4 ± 0.2	Correlates with J-11 and 23P
I	163–200 m [535–656 ft]	Tuff	not dated	Faulted tuff consistent with fissure at Lathrop Wells cone
O	163–188 m [535–617 ft]	Faulted tuff	not dated	Bullfrog Tuff at base
JF6	196 m [643 ft]	Faulted tuff	not dated	Basalt may be deeper, but DOE concluded that basalt encountered below 200 m [656 ft] would be older than 5.3 Ma

*Perry, F., A. Cogbill, R. Kelly, M. Cline, C. Lewis, and R. Fleck. "Status and Interpretation of Aeromagnetic Survey and Drilling Program to Support Probabilistic Volcanic Hazard Analysis–Update." Transcripts of the 172nd Advisory Committee on Nuclear Waste Meeting, Rockville, Maryland, July 17, 2006. ML062090096. pp. 1–164. 2006.
†Ma is million of years before present.

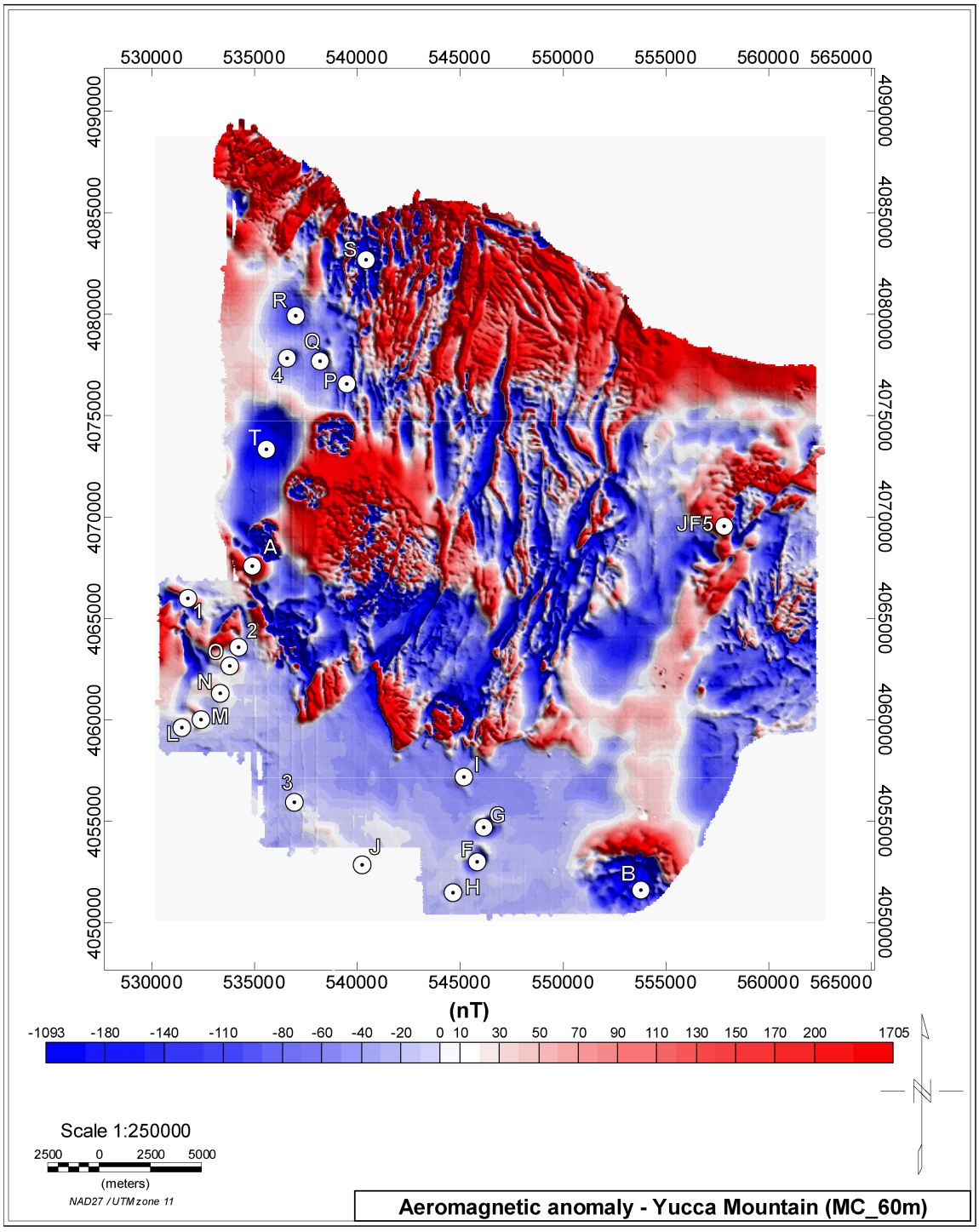

Figure 1-2. Magnetic Anomaly Map Based on Data From DOE Aeromagnetic Survey. Colors Represent Field Intensity Relative to the International Geomagnetic Reference Field. White Circles and Corresponding Letters Identify Anomalies Discussed in Text and in Hill and Stamatakos (2002).

1.2 Purpose and Scope

The purpose of this report is to supplement the analysis provided in Hill and Stamatakos (2002) based on the new DOE aeromagnetic and drilling data. Similar to Hill and Stamatakos (2002), this report provides an independent assessment of existing and new geophysical and geological information to evaluate their effects on the number, ages, and compositions and associated uncertainties of basaltic volcanism in the Yucca Mountain region. In particular, three types of new analyses are discussed in this report:

- Paleomagnetic and rock magnetic analysis on basalt samples was conducted from anomalies A, G, Q, and JF5 to characterize these sources for forward models of the buried basalt bodies. This information also provides information germane to interpretations of the nature of basaltic volcanism that has occurred in the Yucca Mountain region over the past 11 million years.

- Petrographic analysis of representative thin sections of the basalt samples to further characterize the mineralogy and composition of the basalts. Particular attention was paid to thin sections from anomaly A basalts, because a preliminary interpretation of this body suggests it may be a shallow intrusion rather than a buried volcanic lava flow or cinder cone.

- Detailed two-dimensional forward models of the anomalies were constructed to constrain the geometries of the bodies that produced the anomalies and to develop insights into the interpretation of those anomalies not drilled by the DOE drilling program.

In addition to the technical results of these analyses, the report provides the staff with an improved technical basis for understanding the results of the PVHA-U. Review of the results of the PVHA and PVHA-U will be based on the review methods and acceptance criteria in Section 2.2.1.2.2 of the Yucca Mountain Review Plan (NRC, 2003). The review plan describes five aspects staff would review relative to the performance objectives in 10 CFR 63.114. Briefly, these are

(1) Definition of events that may affect compliance
(2) Probability assigned to each event
(3) Conceptual models evaluated and considered to determine probability
(4) Parameters used to calculate the probability
(5) Uncertainty in models and parameters

This report provides staff with information that will be used to support the evaluation of all five review topics. The scope of this review is limited to evaluations of DOE information used in igneous activity probability studies collected since 2002. The report supplements the more comprehensive analysis provided in Hill and Stamatakos (2002).

2 PETROLOGIC, PETROMAGNETIC, AND PALEOMAGNETIC ANALYSES OF BASALT SAMPLES FROM DOE BOREHOLES

2.1 Core Samples

As part of the drilling program, U.S. Department of Energy (DOE) cored the basalt strata encountered in the boreholes drilled at anomalies A, Q, G, and JF5. Staff observed the cores in the Sample Management Facility in May 2006 and requested a set of representative sample splits from each of the four cores. Samples were selected to span the interval of basalt within each core. Fourteen borehole samples were received from the Sample Management Facility, Yucca Mountain Site Characterization Project, and these samples were used for the paleomagnetic, petrographic, and petromagnetic studies described in this report. Each borehole sample was cut into cubic specimens measuring 2 cm [0.8 in] on each side. Samples were cut parallel to the core axis to preserve a consistent sample and specimen orientation relative to the long axis of the cores. DOE did not orient the core azimuth during drilling, and thus the core samples and cube specimens are not oriented with respect to azimuth. There were at least 8 cubes from each of the 14 borehole samples. Details of the core samples and cube subsamples are provided in Tables 2-1 and 2-2. Thin sections were also prepared, 1 for each of the 14 borehole samples.

Table 2-1. Identification of Borehole Core Numbers

Sample Bar Code	Well Identification	Depth Interval (ft.)	Depth Interval (m)	Associated Magnetic Anomaly	Borehole Core Numbers
02043314	USW–VA–1	506.2–506.4	154.3–154.4	A	A1
02043315	USW–VA–1	538.7–538.9	164.2–164.3	A	A2
02043316	USW–VA–1	569.4–569.6	173.6–173.6	A	A3
02043317	USW–VA–1	607.9–608.1	185.3–185.3	A	A4
02043318	USW–VA–1	616.3–616.5	187.8–187.9	A	A5
02043319	USW–VA–4a	484.4–684.6	147.6–147.7	Q	Q1
02043320	USW–VA–4a	512.7–512.9	156.3–156.3	Q	Q2
02043321	USW–VA–4a	533.6–533.8	162.6–162.7	Q	Q3
02043322	UE–25–VA–10	273.3–273.6	83.3–83.4	JF5	JF5–1
02043323	UE–25–VA–10	281.9–282.1	85.9–86.0	JF5	JF5–2
02043324	UE–25–VA–10	307.2–307.4	93.6–93.7	JF5	JF5–3
02043325	USW–VA–2	426.9–427.1	130.1–130.2	G	G1
02043326	USW–VA–2	450.4–450.6	137.3–137.3	G	G2
02043327	USW–VA–2	473.0–473.3	144.2–144.3	G	G3

Table 2-2. Identification of Cube and Thin Section Numbers From Borehole Core Samples		
Borehole Core Numbers	**Cube Sample Numbers for Magnetic Property Measurements**	**Thin Section Sample Numbers**
A1	A1–C1, A1–C2, A1–C3, A1–C4, A1–C5, A1–C6, A1–C7, A1–C8	A1–T1
A2	A2–C1, A2–C2, A2–C3, A2–C4, A2–C5, A2–C6, A2–C7, A2–C8	A2–T1
A3	A3–C1, A3–C2, A3–C3, A3–C4, A3–C5, A3–C6, A3–C7, A3–C8	A3–T1
A4	A4–C1, A4–C2, A4–C3, A4–C4, A4–C5, A4–C6, A4–C7, A4–C8	A4–T1
A5	A5–C1, A5–C2, A5–C3, A5–C4, A5–C5, A5–C6, A5–C7, A5–C8	A5–T1
Q1	Q1–C1, Q1–C2, Q1–C3, Q1–C4, Q1–C5, Q1–C6, Q1–C7, Q1–C8	Q1–T1
Q2	Q2–C1, Q2–C2, Q2–C3, Q2–C4, Q2–C5, Q2–C6, Q2–C7, Q2–C8	Q2–T1
Q3	Q3–C1, Q3–C2, Q3–C3, Q3–C4, Q3–C5, Q3–C6, Q3–C7, Q3–C8	Q3–T1
JF5–1	JF5–1–C1, JF5–1–C2, JF5–1–C3, JF5–1–C4, JF5–1–C5, JF5–1–C6, JF5–1–C7, JF5–1–C8	JF5–1–T1
JF5–2	JF5–2–C1, JF5–2–C2, JF5–2–C3, JF5–2–C4, JF5–2–C5, JF5–2–C6, JF5–2–C7, JF5–2–C8	JF5–2–T1
JF5–3	JF5–3–C1, JF5–3–C2, JF5–3–C3, JF5–3–C4, JF5–3–C5, JF5–3–C6, JF5–3–C7, JF5–3–C8	JF5–3–T1
G1	G1–C1, G1–C2, G1–C3, G1–C4, G1–C5, G1–C6, G1–C7, G1–C8	G1–T1
G2	G2–C1, G2–C2, G2–C3, G2–C4, G2–C5, G2–C6, G2–C7, G2–C8	G2–T1
G3	G3–C1, G3–C2, G3–C3, G3–C4, G3–C5, G3–C6, G3–C7, G3–C8	G3–T1

2.2 Thin-Section Petrography

The major mineral phases present within each of 14 thin sections were identified through a microscope in both plane-polarized and cross-polarized light. Modal percentages of the main mineral phases were then determined from statistical point counts. The surface area of each thin section was divided into a grid with a 1-mm [0.04-in] spacing. Using a vernier-scale mechanical stage and polarized light, mineral identifications were made directly beneath the cross hairs of the ocular for each 1-mm [0.04-in] increment. The percentages of each mineral

present were approximated using ≥150 point counts per thin section. Alteration products and other diagenetic materials were also reported in the characterization of the samples.

Each individual mineral grain reported during point counting was identified as groundmass or phenocryst so that the ratio of these textural components could be calculated. As the size of mineral grains belonging to groundmass is variable between samples, grains exceeding the mean grain size of groundmass crystals by 100 µm [0.004 in] or more were reported as phenocrysts. A brief description was then given for each thin section based upon groundmass crystallinity, grain size of groundmass minerals, and other observed textural features. Tables 2-3 through 2-6 summarize the results of the thin-section analysis. Representative photomicrographs are provided in Figure 2-1.

All anomaly samples are holocrystalline, basalt porphyrys, though groundmass grain size, phenocryst percentage, volcanic textures, and relative mineral abundance vary between them. Anomaly A has a much finer groundmass than the others, with the majority of grains being microlites. Anomaly JF5 has a very coarse texture relative to the other anomalies, with the size of groundmass grains frequently exceeding the size of phenocrysts within anomaly A. The size of grains composing the groundmass of samples G and Q is intermediate, with similar amounts of microlites and microphenocrysts. Phenocryst percentages range between 12 and 34 percent, with an overall mean of 23 ± 7 percent.[4] In contrast, samples from anomaly A have an average of 31 ± 2 percent phenocrysts. In addition, anomaly A samples often contain coarse-grained zones similar to the coarse pods of syenite found in the sills at Paiute Ridge (Valentine and Krogh, 2006).

Three distinct volcanic textures were observed within the thin sections of the four magnetic anomalies. A recurring glomeroporphyritic texture was seen throughout the thin sections prepared from anomaly A and appears as radial aggregates of augite phenocrysts. Anomalies A, G, and JF5 display strong trachytoid textures resulting from the alignment of elongate plagioclase grains parallel to the direction of fluid flow. Vesiculation was observed in thin sections of anomaly JF5 and was most pronounced in JF5-1, which was taken from the borehole nearest the surface. Plagioclase feldspar is a dominant phase within all of the thin sections, and augite is abundant in anomalies A, G, and JF5. Anomaly G shows presence of hornblende. Anomaly Q has olivine (or olivine altered to iddingsite) as the second most common phase to plagioclase. Common accessory minerals include magnetite, iddingsite, and biotite, which is unique to anomaly A.

[4]Note that these reported errors are standard deviations of point counts and do not include any counting errors due to the relatively small number of point counts conducted.

Table 2-3. Thin Section Point Counts for Anomaly A												
	Count	Percentage	Count	Percentage	Count	Percentage	Count	Percentage	Count	Percentage	Average Percentage	Standard Deviation
Thin Section	**A1–T1**		**A2–T1**		**A3–T1**		**A4–T1**		**A5–T1**			
Groundmass	242	66	301	70	317	69	323	70	362	72	69	2
Phenocrysts	124	34	130	30	143	31	141	30	142	28	31	2
Augite	143	31	183	40	159	32	193	37	271	52	38	8
Plagioclase	85	18	115	25	147	30	116	22	129	25	24	4
Iddingsite	81	17	81	18	90	18	94	18	36	7	16	5
Olivine	0	0	0	0	0	0	0	0	13	3	1	1
Biotite	11	2	4	1	11	2	9	2	8	2	2	1
Magnetite	46	10	48	10	53	11	52	10	47	9	10	1
Clays	0	0	0	0	0	0	0	0	0	0	0	0
Diagenetic	99	21	31	7	38	8	60	12	20	4	10	7
Voids	0	0	0	0	0	0	0	0	0	0	0	0
Total	465	100	462	100	498	100	524	100	524	100		

Table 2-4. Thin Section Point Counts for Anomaly G								
	Count	Percentage	Count	Percentage	Count	Percentage	Average Percentage	Standard Deviation
Thin Section	**G1–T1**		**G2–T1**		**G3–T1**			
Groundmass	144	88	140	85	141	83	86	3
Phenocrysts	19	12	24	15	28	17	14	3
Augite	25	14	24	14	41	23	17	5
Plagioclase	116	66	112	63	94	53	61	7
Iddingsite	3	2	16	9	16	9	7	4
Olivine	3	2	0	0	5	3	2	1
Biotite	0	0	0	0	0	0	0	0
Magnetite	16	9	12	7	13	7	8	1
Clays	11	6	13	7	7	4	6	
Diagenetic	1	1	0	0	0	0	0	0
Voids	0	0	0	0	0	0	0	0
Total	175	100	177	100	176	100		

Table 2-5. Thin Section Point Counts for Anomaly JF5								
	Count	Percentage	Count	Percentage	Count	Percentage	Average Percentage	Standard Deviation
Thin Section	**JF5–1–T1**		**JF5–2–T1**		**JF5–3–T1**			
Groundmass	188	84	201	83	151	71	80	8
Phenocrysts	35	16	37	17	61	29	20	8
Augite	42	17	34	23	38	16	16	1
Plagioclase	131	52	154	53	124	52	56	7
Iddingsite	32	13	32	9	35	15	14	1
Olivine	1	0	4	3	0	0	1	1
Biotite	0	0	0	0	0	0	0	0
Magnetite	17	7	14	6	15	6	6	0
Clays	0	0	0	0	0	0	0	0
Diagenetic	0	0	0	0	20	8	3	5
Voids	31	12	2	1	7	3	5	6
Total	254	100	240	100	239	100		

Table 2-6. Thin Section Point Counts for Anomaly Q								
	Count	Percentage	Count	Percentage	Count	Percentage	Average Percentage	Standard Deviation
Thin Section	**Q1–T1**		**Q2–T1**		**Q3–T1**			
Groundmass	183	79	143	76	124	74	76	2
Phenocrysts	49	21	46	24	43	26	24	2
Augite	33	14	5	3	8	5	7	6
Plagioclase	146	61	119	62	100	58	60	2
Iddingsite	42	18	32	17	26	15	16	1
Olivine	0	0	0	0	6	4	1	2
Biotite	0	0	0	0	0	0	0	0
Magnetite	11	5	33	17	27	16	12	7
Clays	0	0	0	0	0	0	0	0
Diagenetic	8	3	4	2	6	4	3	1
Voids	0	0	0	0	0	0	0	0
Total	240	100	193	100	173	100		

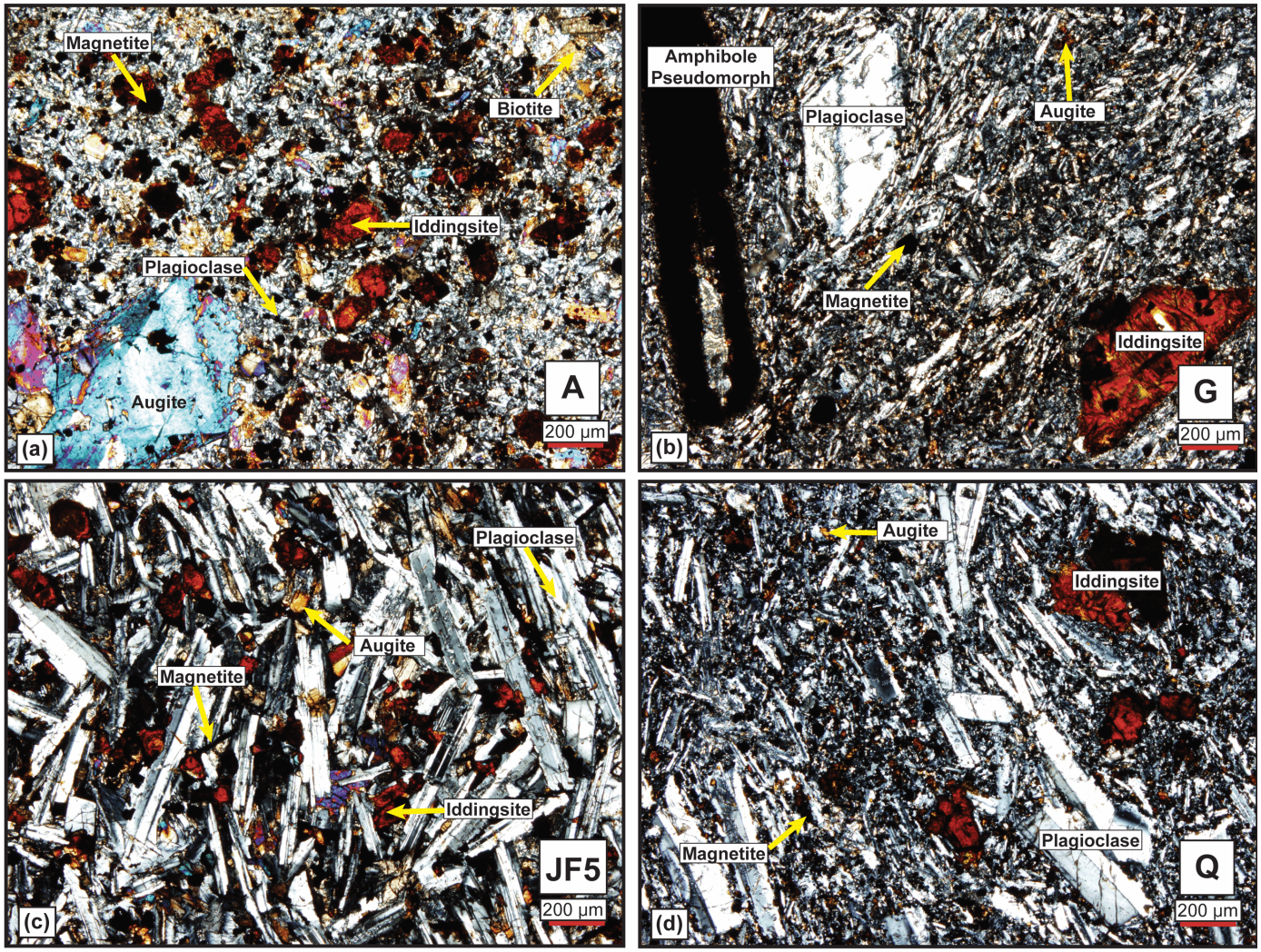

Figure 2-1. Representative Thin Sections in Polarized Light for Anomalies (a) A, (b) G, (c) JF5, and (d) Q

2.3 Magnetic Data

2.3.1 Laboratory Methods

Laboratory measurements were performed at the Institute of Rock Magnetism, which is located at the University of Minnesota in Minneapolis, Minnesota. The measurements were designed to characterize the magnetic properties of the samples as input to the forward modeling of the anomalies discussed in Section 3 of this report. The set of experiments included measurements of (i) natural remanent magnetization, (ii) alternating field demagnetization and thermal demagnetization to isolate the inclination of the characteristic remanent magnetization, (iii) room-temperature bulk susceptibility, (iv) temperature dependence of low-field susceptibility to 700 °C [1,292 °F], and (v) hysteresis and coercivity. Dunlop and Özdemir (1997) and Evans and Heller (2003) describe the methods used in the measurements. Note that because the cores were not oriented with respect to core azimuth, the full description of the characteristic remanent magnetization vector (inclination and declination) could not be obtained.

Remanent magnetizations were measured on a three-axis cryogenic magnetometer. Susceptibility was measured on a Kappabridge at room temperature. The Kappabridge was also used in the temperature-sweep mode to measure susceptibility as a function of temperature over heating and cooling cycles from 20 to 700 °C [68 to 1,292 °F] to determine the Curie temperature of 1 sample from each of the 14 core samples. Hysteresis and coercivity measurements were made on a Vibrating Sample Magnetometer at room temperature. Alternating field demagnetizations were conducted using 14 steps of progressively increasing alternating fields from 5 to 200 mT. Thermal demagnetization was conducted using a standard paleomagnetic furnace with a rest field of less than 100 nT. Samples were demagnetized in 16 progressive temperature steps from 20 to 700 °C [68 to 1,292 °F].

2.3.2 Results of Laboratory Measurements

Remanent Magnetization. Most of the samples exhibited intensities of natural remanent magnetization between 0.5 and 2.0 A/m, although samples from lower portions of the JF5 anomaly core yielded intensities as high as 4.2 A/m (Figure 2-2). Inclination angles for the natural remanent magnetization were of both polarities (Figure 2-3). Samples from anomaly A showed positive Z, or normal-polarity magnetization, with inclination angles that appear to become progressively shallower with depth in the core from 56° to 42° (Table 2-1). Samples from anomaly G showed negative, or reversed-polarity inclinations, that ranged between approximately −50° and −70°. Samples from the anomaly JF5 core showed normal-polarity inclinations that also appeared to shallow down core from approximately 38° to 24°. Samples from anomaly Q showed both normal- and reversed-polarity inclinations. Reversed-polarity inclinations are observed in the upper two core samples, with shallow inclination angles of −10° to −27°. Normal-polarity inclinations are observed in the lower core sample, with an average inclination angle of 55°.

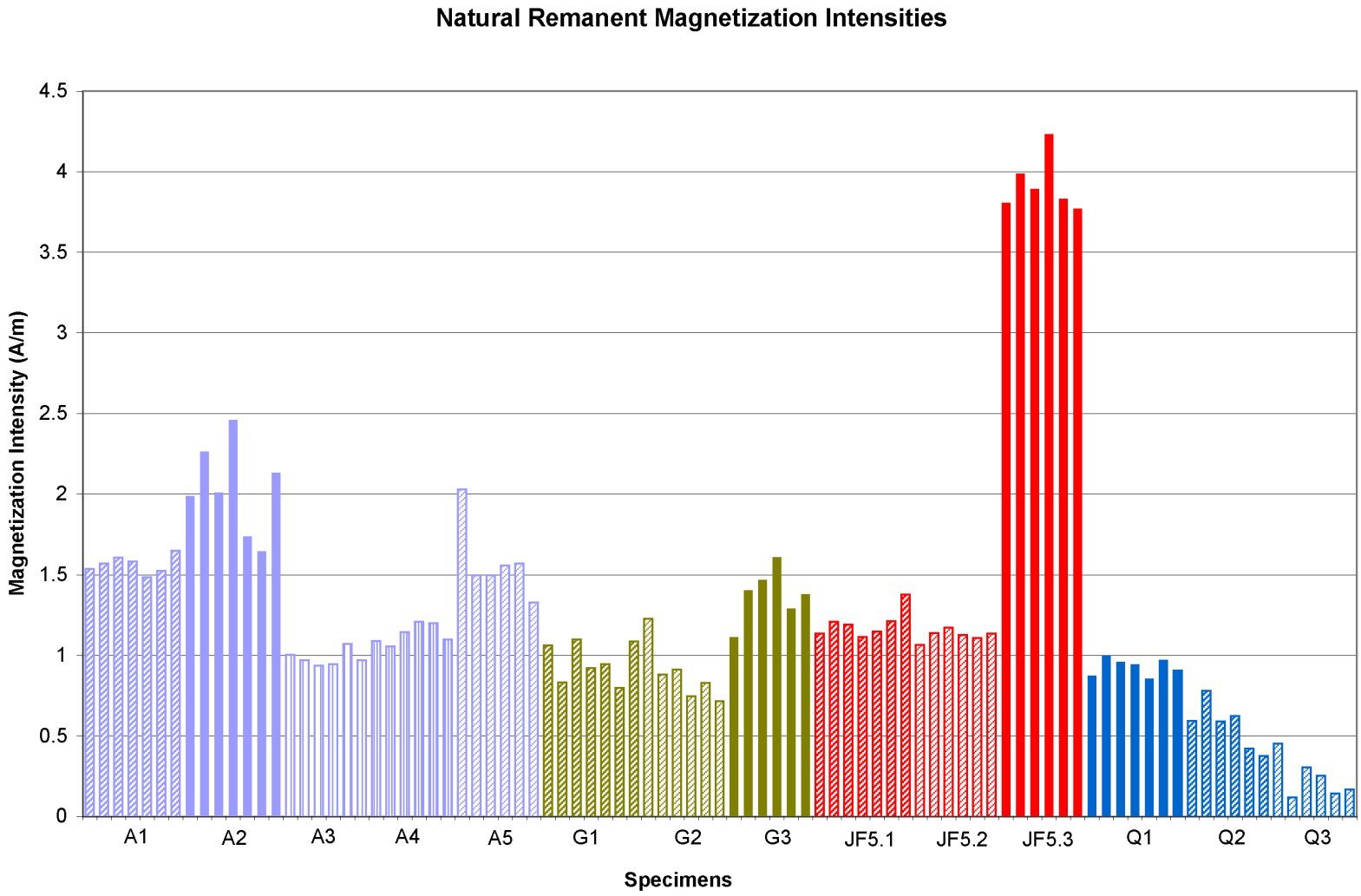

Figure 2-2. Results From Natural Remanent Magnetization Measurements for Basalt Specimens From Anomalies A, G, JF5, and Q

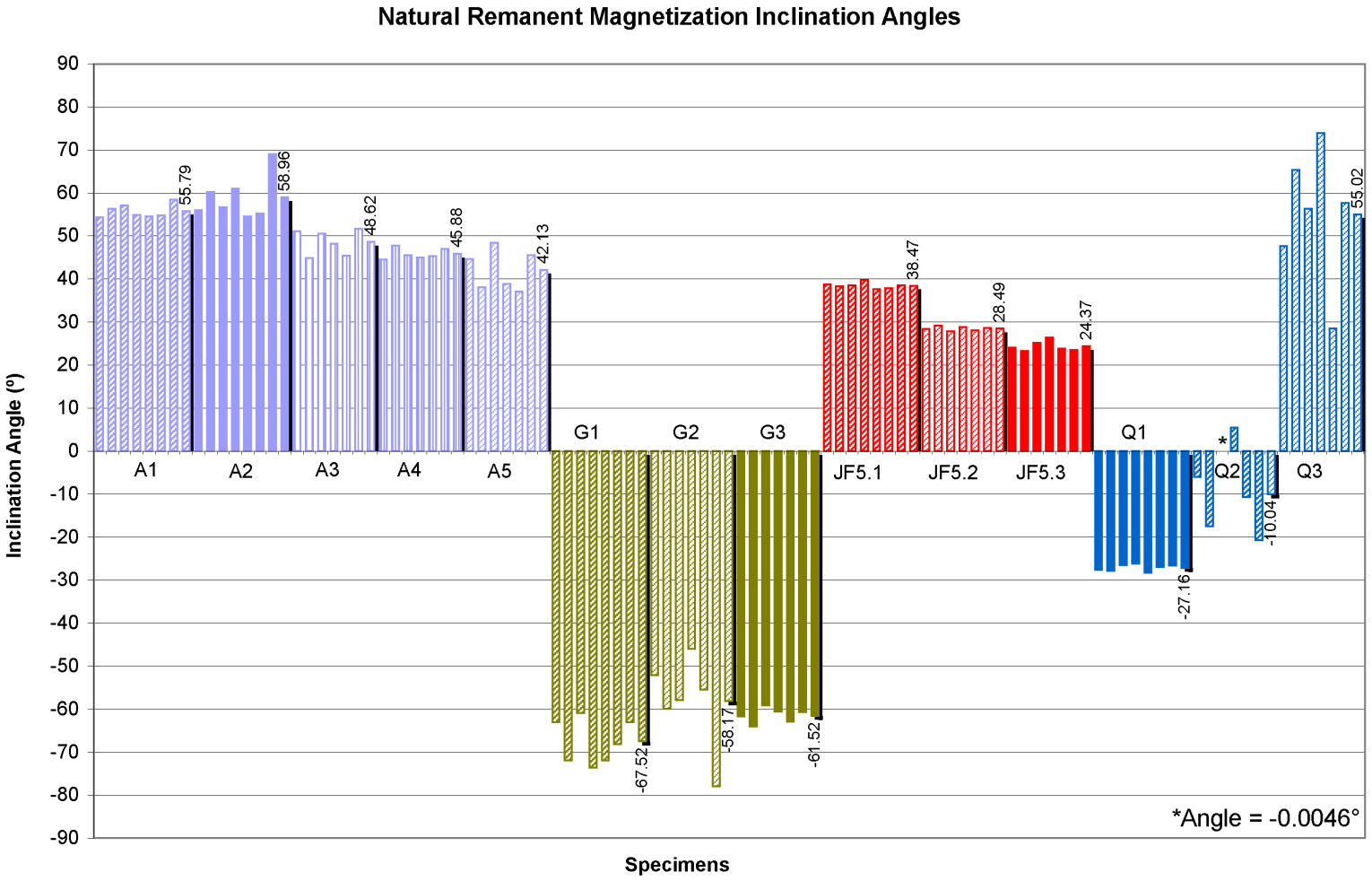

Figure 2-3. Results From Inclination Only Statistics of Natural Remanent Magnetization for Basalt Specimens From Anomalies A, G, JF5, and Q. Bars with Shadows Denote the Estimated Inclination Angles for Specific Anomaly Specimens.

During both thermal and alternating-field demagnetization, most samples showed stable univectorial decay of the natural remanent magnetization to the origin (Figure 2-4). Many of the samples, especially those from the anomaly A core, had high coercivities, with mean destructive fields often greater than 50 mT and incomplete cleaning in fields as high as 200 mT. Thermal demagnetization also showed univectorial decay of the natural remanent magnetization with distributed unblocking between 400 and 600 °C [752 and 1,112 °F]. The exceptions to the well-behaved demagnetization were specimens from the lower two samples in the core from anomaly Q. In these samples, demagnetization was incoherent and unstable (Figure 2-4c). Although characteristic directions were derived from these samples, the directions did not trend to the origin, and the associated mean angular deviations were large (Figure 2-5).

Characteristic remanent magnetizations isolated during thermal and alternating-field demagnetization were determined from visual inspection of linear segments of the vector endpoint diagrams. Directions were determined from a least-square fit to the observed linear trajectories of the endpoint diagrams (e.g., Kirschvink, 1980). With the noted exceptions from the lower two core samples from the core at anomaly Q, mean angular deviations were generally smaller than 5.0° (Figure 2-5). Individual sample inclinations were combined to sample core mean directions (Table 2-7) using the inclination-only method of McFadden and Reid (1982). Inclinations from the characteristic magnetizations were similar to the natural remanent magnetization data (Figure 2-3).

Susceptibility. Volume susceptibility values are more varied than the intensities of the natural remanent magnetizations, ranging between approximately 5×10^{-4} and 3.5×10^{-3} SI (Figure 2-6). With the exception of samples from the anomaly Q core, Königsberger ratios are large, ranging between approximately 10 and 70 (Figure 2-7).

Curie Temperatures and Magnetic Mineralogy. Temperature dependence of low-field susceptibility showed reversible heating and cooling curves dominated by a single magnetic phase with a narrow curie temperature band between 500 and 580 °C [932 and 1,076 °F] (Figure 2-8). Curie temperatures, determined from the maximum curvature in the thermomagnetic curves, are between 508 and 581 °C [946 and 1,078 °F] for all samples except the sample from JF5-3 (Table 2-8). These curie temperatures are close to those of magnetite and strongly suggest that magnetite is the dominant magnetic phase in most samples. Heating curves above 600 °C [1,112 °F] are near zero, and thus there is little contribution from hematite. The exception is JF5-3, which had a Curie temperature of 626 °C [1,159 °F] indicating hematite is also present. In a few of the samples, there is also a minor bump at about 320 °C [608 °F], suggesting a small fraction of either pyrhotite or titanomagnetite.

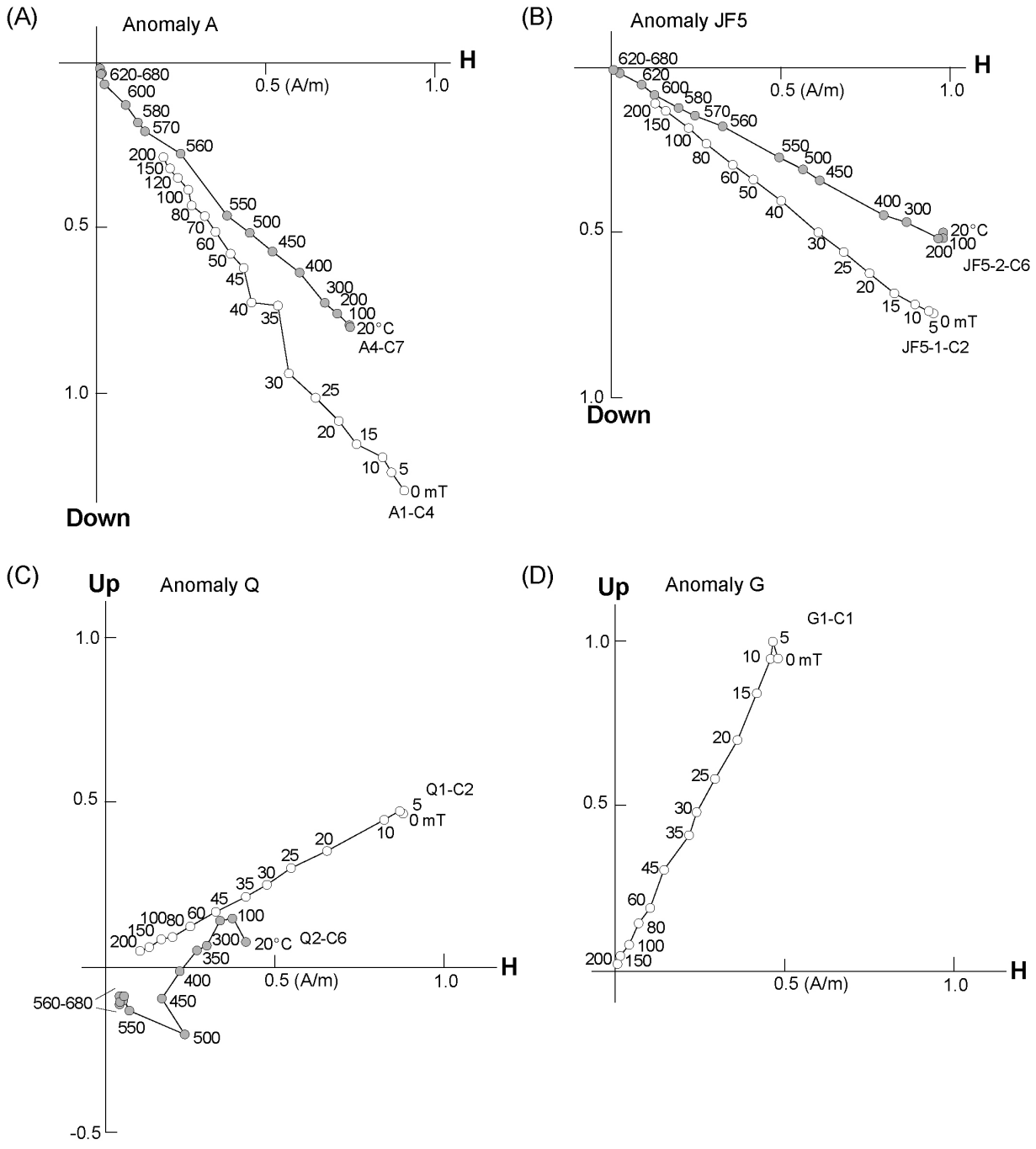

Figure 2-4. Sample Vector Endpoint Demagnetization Diagrams Showing Thermal (Black Circles) and Alternating Field (White Circles) Demagnetization of Basalt Samples. Diagrams Plot the Z-Component as a Function of the Horizontal Component.

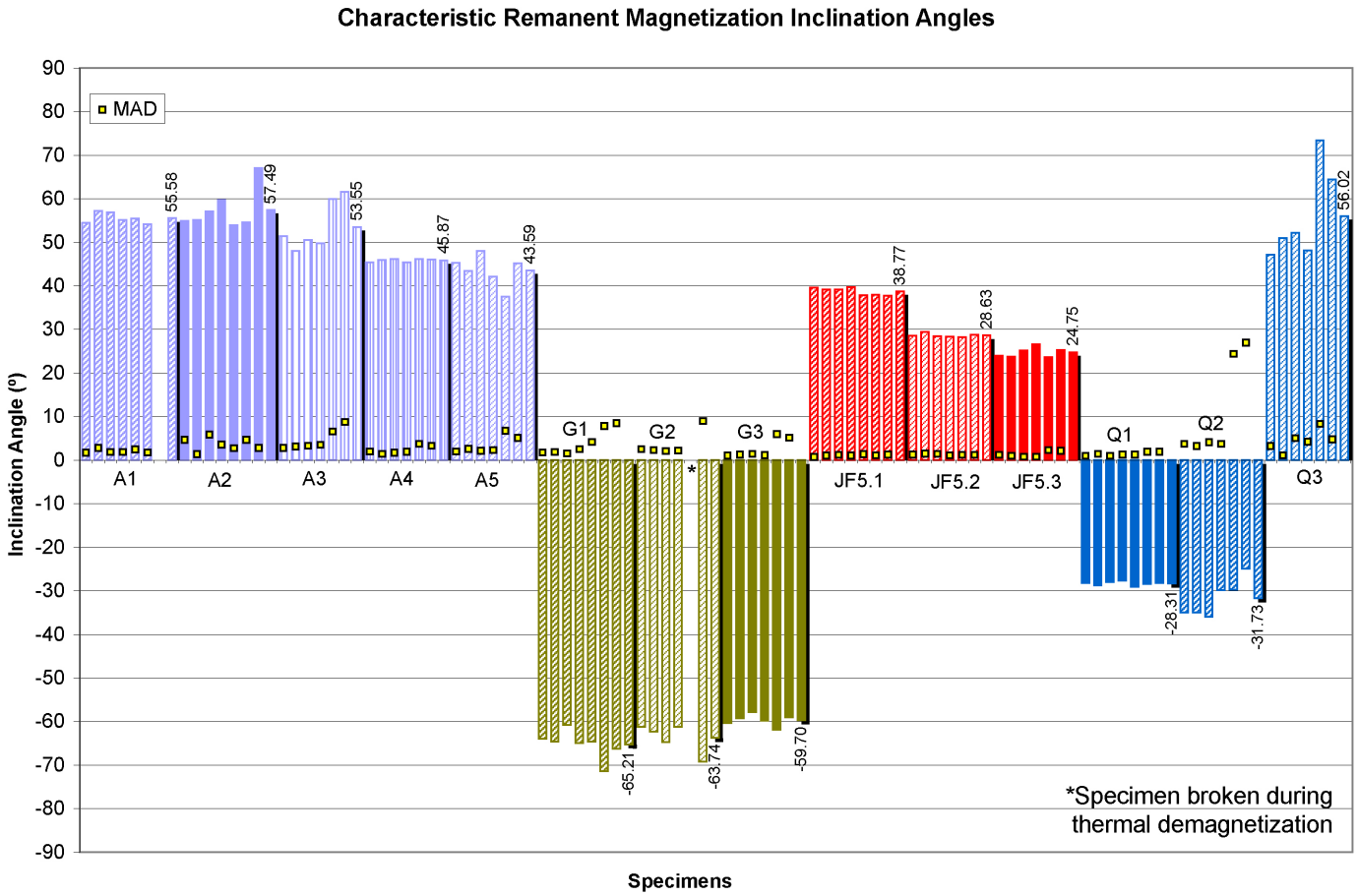

Figure 2-5. Results From Inclination Only Statistics of Characteristic Remanent Magnetization for Basalt Specimens After Demagnetization From Anomalies A, G, JF5, and Q. Bars With Shadows Denote Estimated Characteristic Inclination Angles for Specific Anomaly Specimens. MAD—Mean Angular Deviation.

Table 2-7. Summary of Inclination Data From Borehole Samples						
Core Sample	**Natural Remanent Magnetization**			**Characteristic Remanent Magnetization**		
	Inc.*	**Kappa†**	**alpha-95‡**	**Inc.**	**Kappa**	**alpha-95**
A1	55.8	1,345.0	1.4	55.6	2,075.0	1.3
A2	59.0	128.5	4.7	57.5	151.7	4.3
A3	48.6	378.0	3.1	53.5	100.2	6.0
A4	45.9	2,124.1	1.3	45.9	24,006.9	0.4
A5	42.1	148.6	4.9	43.6	258.2	3.7
G1	−67.5	122.2	4.8	−65.2	320.9	3.0
G2	−58.2	27.5	11.7	−63.7	287.4	4.2
G3	−61.5	1,065.5	1.8	−59.7	1,766.7	1.4
JF5–1	38.5	6,730.1	0.6	38.8	4,507.0	0.8
JF5–2	28.5	15,642.3	0.5	28.6	19,383.2	0.4
JF5–3	24.4	2,305.5	1.3	24.7	2,562.0	1.2
Q1	−27.2	5,223.0	0.7	−28.3	13,468.6	0.5
Q2	−10.0	53.4	8.3	−31.7	178.1	4.5
Q3	55.0	12.9	17.3	56.0	29.2	11.3

*Inc., or inclination, is the average inclination of the core sample based on the mean of the individual specimens.
†Kappa is the Fisher precision parameter (Fisher, 1953)§ and is a measure of the concentration of the specimen directions.
‡Alpha-95 is the angular deviation that represents the 95-percent confidence interval about the mean.
§Fisher, R.A. "Dispersion on a Sphere." *Proceedings of the Royal Astronomical Society of London. Series A.* Vol. 217. pp. 295–305. 1953.

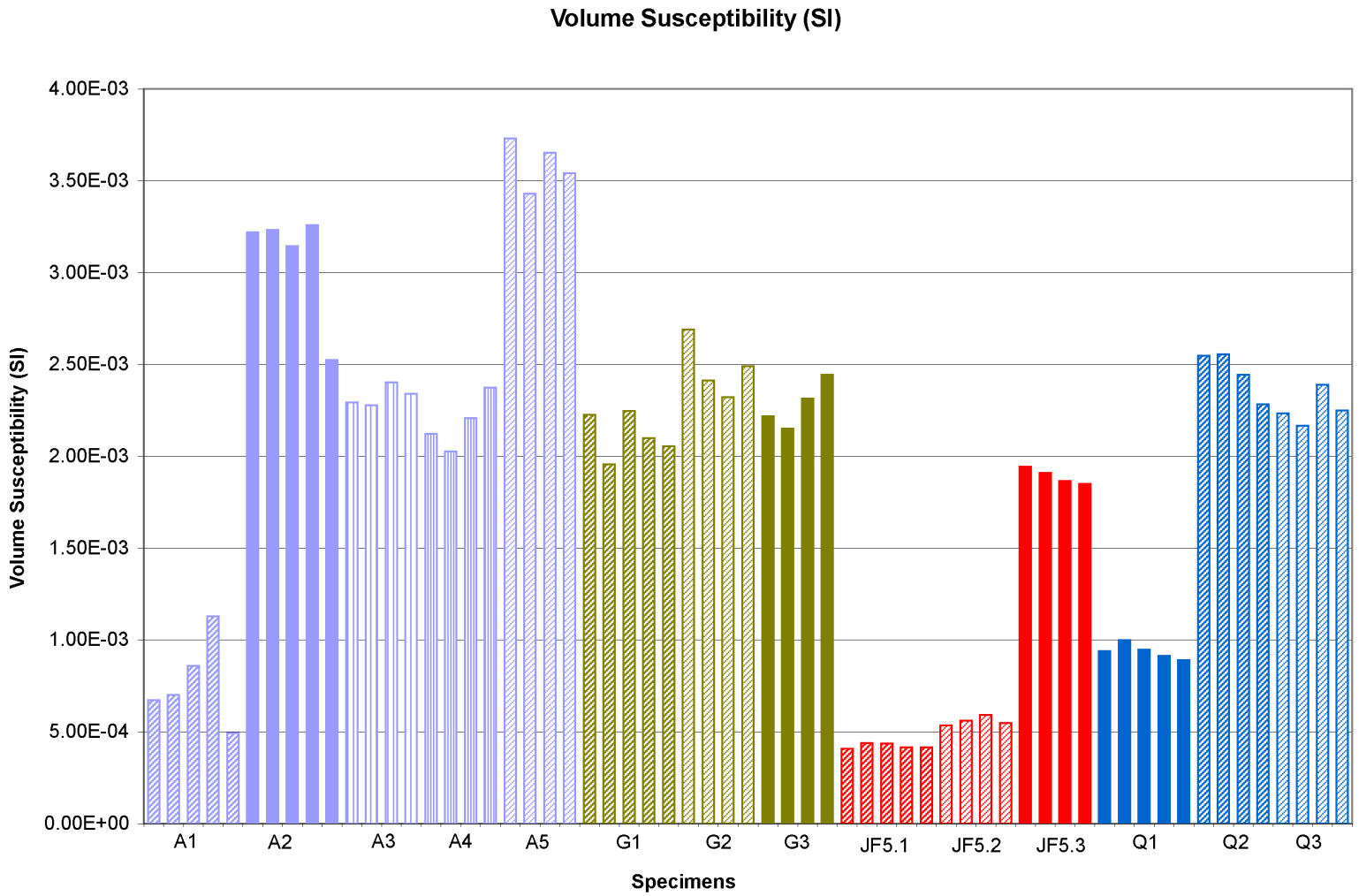

Figure 2-6. Results From Volume Susceptibility Measurements for Basalt Specimens From Anomalies A, G, JF5, and Q

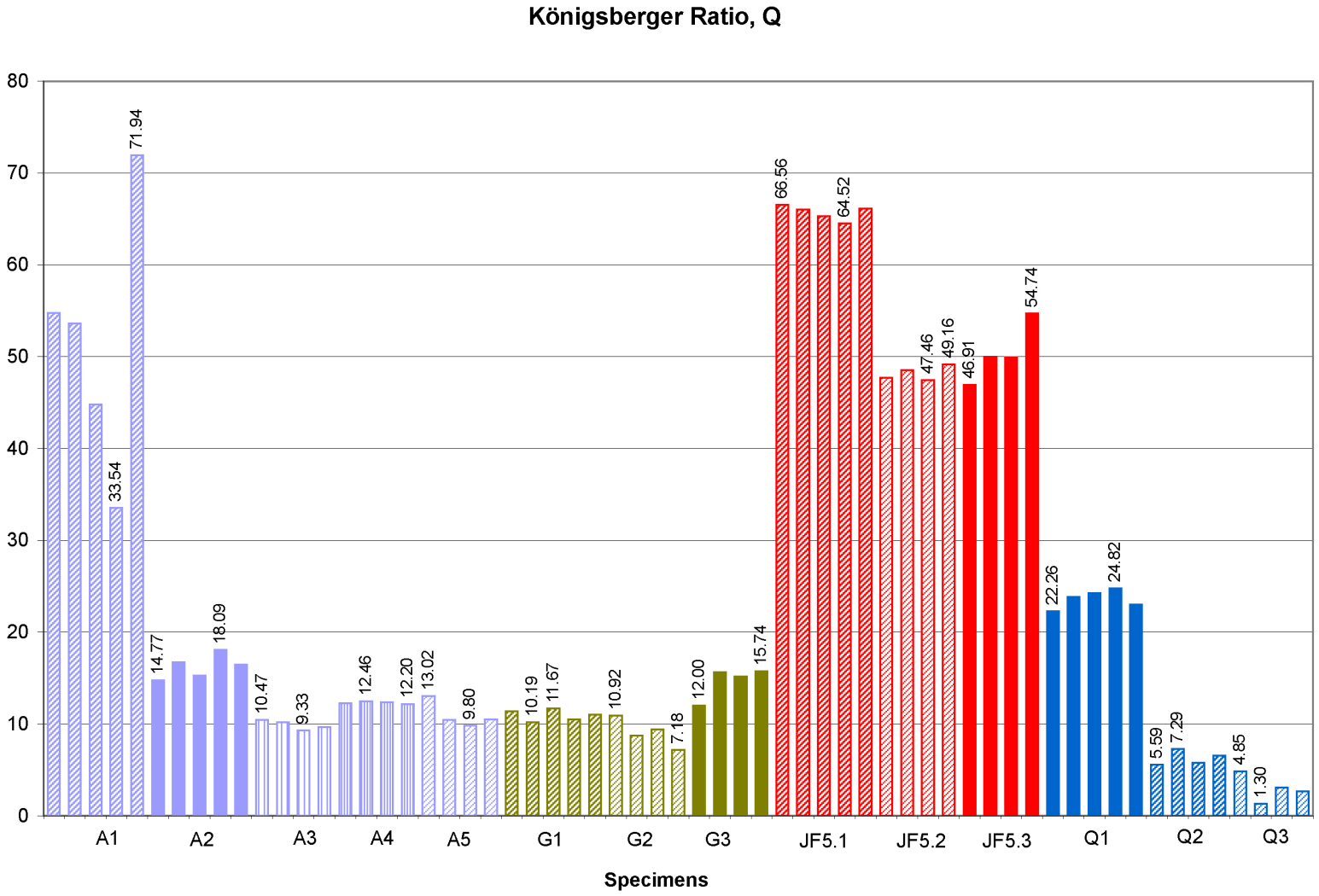

Figure 2-7. Results of Königsberger Ratio (Q) for Basalt Specimens From Anomalies A, G, JF5, and Q

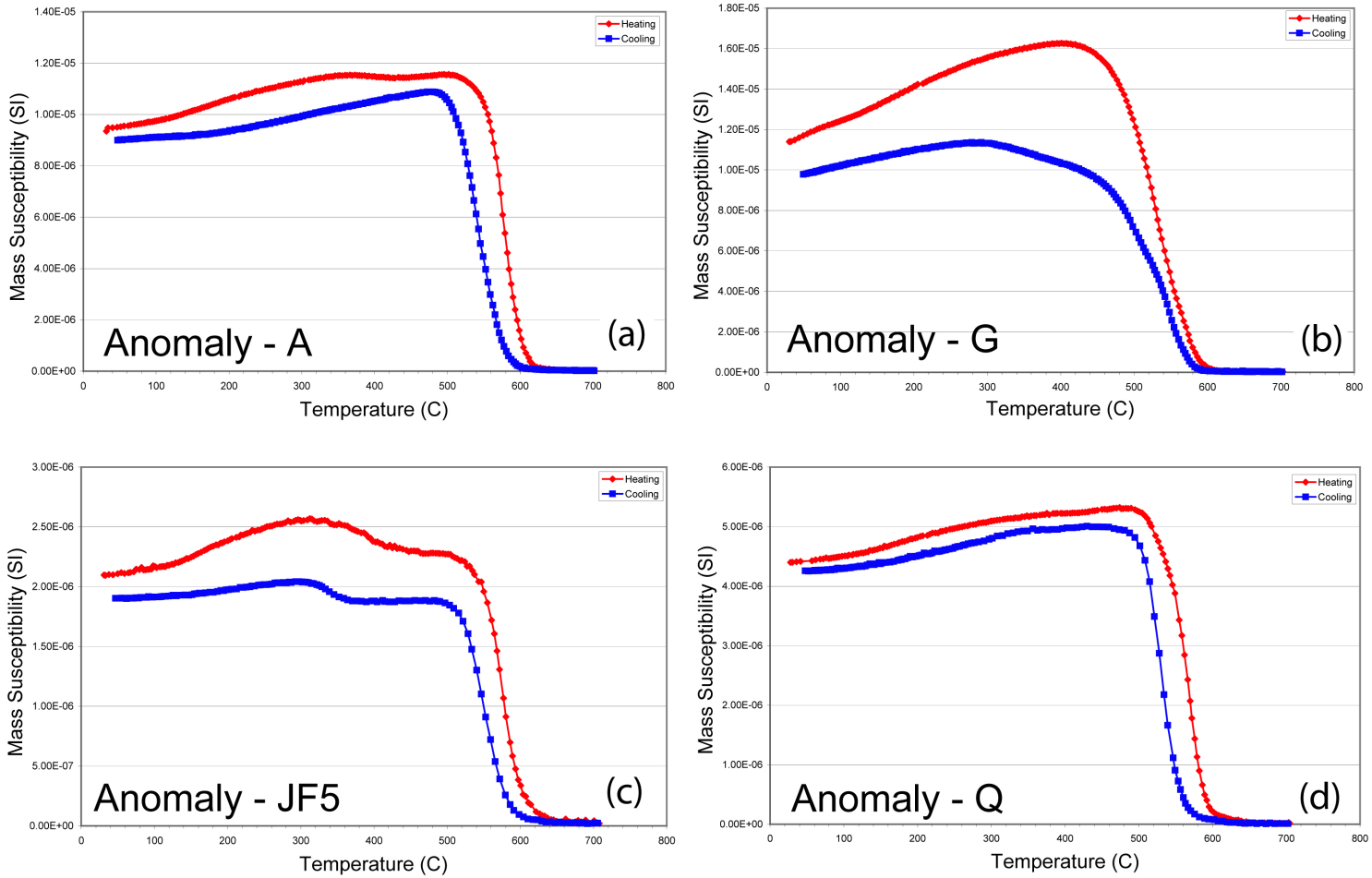

Figure 2-8. Representative Results From Temperature Dependence of Low-Field Susceptibility Measurements for Anomalies (a) A, (b) G, (c) JF5, and (d) Q. Red Curves Are Heating Cycle; Blue Curves Are Cooling Cycle.

Table 2-8. Curie Temperatures From Measurements of Temperature-Dependent Low-Field Susceptibility		
Core Sample	**Curie Temperature (°C)**	**Curie Temperature (°F)**
A1	573.1	1,063.6
A2	570.8	1,059.4
A3	578.5	1,073.3
A4	574.6	1,066.3
A5	559.5	1,039.1
G1	508.4	947.1
G2	540.2	1,004.4
G3	524.8	976.6
JF5–1	581.4	1,078.5
JF5–2	578.7	1,073.7
JF5–3	625.7	1,158.3
Q1	570.8	1,059.4
Q2	523.8	974.8
Q3	544.0	1,011.2

Hysteresis results obtained from the Vibrating Sample Magnetometer are summarized in the Day Plot (Day, et al., 1977) shown in Figure 2-9. Ratios of saturation remanence (M_{rs}) to saturation magnetization (M_s) range from 0.05 to 0.4. Ratios of coercivity of remanence (H_{cr}) to coercivity (H_c) range from 1.5 to 3.0. The data are well clustered within the pseudosingle domain field for magnetite.

2.3.3 Interpretation of Petrographic and Magnetic Data

The data show that all the basalt samples carry a strong remanent magnetization that dominates over susceptibility, as evident from the large Königsberger ratios. Thus the natural remanent magnetization intensities and inclinations represent the best estimates of the magnetic parameters that should be used to model the anomalies. Table 2-9 summarizes the values used for the forward models based on these results.

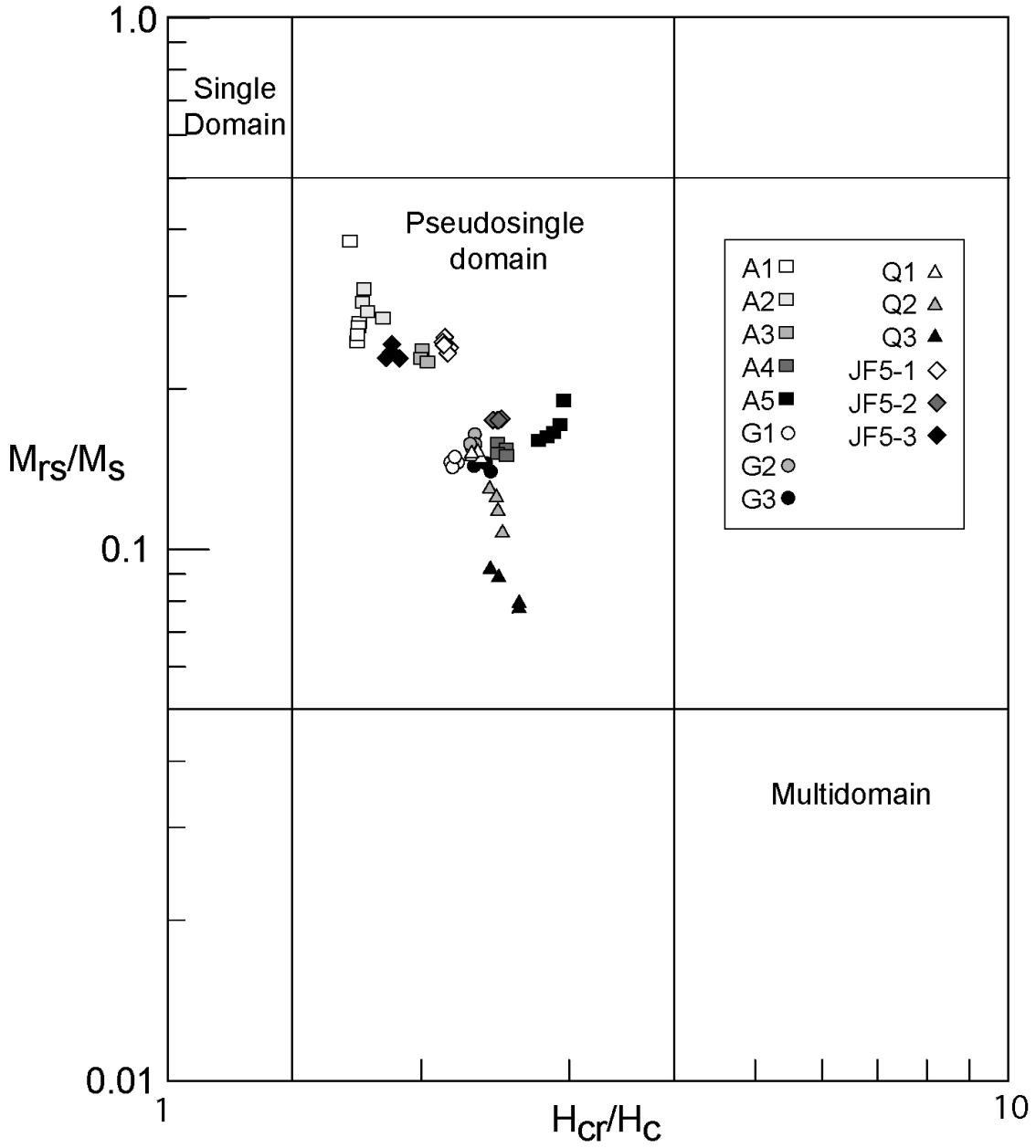

Figure 2-9. Results of Hysteresis Experiments on a Day Plot. Data for Individual Specimens Are Well Clustered. All Samples Plot in the Pseudosingle Domain Field for Magnetite.

Table 2-9. Source Parameters for Magnetic Anomaly Models					
Anomaly	**Unit**	**χ* (SI)**	**Inc† (°)**	**Dec‡ (°)**	**M§ (A/m)**
A	Quaternary Alluvium (Qal)	0	–	–	0
	Basalt	0.003	59°	0°	2.46
	Ammonia Tanks (Tma)	0	59°	0°	0.58
	Rainier Mesa (Tmr)	0	−55°	168°	2.7
G	Quaternary Alluvium (Qal)	0	–	–	0
	Basalt	0.003	−68°	0°	1.61
JF5	Quaternary Alluvium (Qal)	0	–	–	0
	Basalt	0.002	38°	0°	4.23
Q	Quaternary Alluvium (Qal)	0	–	–	0
	Basalt	0.001	−27°	180°	0.99
	Ammonia Tanks (Tma)	0	59°	0°	0.58
	Rainier Mesa (Tmr)	0	−55°	168°	2

*χ is the volume susceptibility.
† Inc is the inclination angle of the remanent magnetization vector.
‡ Dec is the declination angles of the remanent magnetization vector with respect to north. Note that in the absence of measured declinations, declinations were assumed to be north for normal-polarity inclinations and south for reversed-polarity inclinations.
§ M is intensity of the remanent magnetization.

Remanence intensities of the basalts are orders of magnitude larger than the magnetization intensities of alluvial material and Paleozoic bedrock, and thus the magnetic anomalies in areas away from Miocene tuff bedrock (e.g., Amargosa Desert) can be adequately modeled using single body sources of highly magnetic basalt surrounded by nonmagnetic material. In contrast, the magnetization intensities and susceptibilities of the basalt samples are quite similar to those of many of the tuff units that compose Yucca Mountain (e.g., Rosenbaum and Snyder, 1985) in the areas of exposed bedrock north and east of Yucca Mountain. Thus, models of basalt bodies in these regions are more complex and uncertain. As discussed at length in Hill and Stamatakos (2002), detection of basaltic features within these regions therefore remains obscured by the complex patterns of magnetic anomalies produced by faulted tuff. Past episodes of basaltic volcanism may remain present but undetected in regions with complex aeromagnetic patterns arising from the tuff exposures, or in areas with faulted tuff in the shallow subsurface.

Observations from thin sections, demagnetization data, and magnetic properties from rock magnetic experiments also suggest that, with the possible exceptions from the lower two samples in the core from anomaly Q, basalt samples preserve thermo-remanent magnetizations that were acquired when the basalts were initially emplaced and cooled. The magnetite is fine grained, and its pseudosingle domain character makes it ideal to preserve an ancient magnetic field. Demagnetization of the samples shows little evidence for thermo-chemical or viscous remanent magnetization overprints. Thus, the recorded polarity in conjunction with the Geomagnetic Polarity Time Scale (Cande and Kent, 1995) provides an important constraint on the isotopic dates used to estimate the ages of the basalt samples from the drill cores.

The remanent magnetizations also suggest that the basalt bodies associated with anomalies A, Q, and JF5 are not uniformly magnetized, and thus these features may represent a more complex volcanic and geologic setting. The remanence inclinations from anomaly Q appear to record a reversal of the magnetic field between samples from Q2 and Q3. However, because of the poor quality of the demagnetizations from Q, no definitive conclusions can be made about this apparent reversal.

In addition to the possible reversal in Q, the characteristic inclinations for samples from anomalies Q, JF5, and the lower parts of the core at anomaly A are shallower than the reference 58° ± 3° inclination for this latitude of North America over the past 11 million years (Hagstrum, et al., 1987). These shallow inclinations represent acquisition of the characteristic remanent magnetization over a time interval that was too short to average secular variation of the geomagnetic field, or the lava flows were rotated about a horizontal axis due to faulting and fault-block tilting. Unfortunately, there is not enough information available to resolve this question. The lack of declination data for the characteristic remanent magnetization precludes a more comprehensive structural assessment to test whether the shallow inclinations are the result of tilting of the basalt bodies due to faulting.

Finally, textural and mineralogical observations from the cores offer additional insights into the nature of basaltic volcanism in Crater Flat. First, the presence of hydrous phases, including the observation of relict textures indicative of resorbed and reacted amphibole (Anomaly G in Figure 2-1) supports the interpretation of previous studies that some of the basalt melts in Crater Flat were equilibrated at near-water-saturated conditions during their ascent (e.g., Nicholis and Rutherford, 2004). Second, the biotite observed in core samples from anomaly A appears to be fresh and lacks the red-brown pleochroism characteristic of oxybiotite associated with erupted lava flows in Crater Flat (e.g., Vaniman, et al., 1982). Instead the biotite appears to have brown-green pleochrosim more typical of a slow-cooled, stable, intrusive biotite generally found in more intermediate composition diorites.